Fabrication of pillar-array superhydrophobic silicon surface and thermodynamic analysis on the wetting state transition*

Liu Si-Si(刘思思), Zhang Chao-Hui(张朝辉)†, Zhang Han-Bing(张寒冰), Zhou Jie(周 杰), He Jian-Guo(何建国), and Yin Heng-Yang(尹恒洋)

School of Mechanical, Electronic and Control Engineering, Beijing Jiaotong University, Beijing 100044, *China*

(Received 11 November 2012; revised manuscript received 3 May 2013)

Textured silicon (Si) substrates decorated with regular microscale square pillar arrays of nearly the same side length, height, but different intervals are fabricated by inductively coupled plasma, and then silanized by self-assembly octadecyltrichlorosilane (OTS) film. The systematic water contact angle (CA) measurements and micro/nanoscale hierarchical rough structure models are used to analyze the wetting behaviors of original and silanized textured Si substrates each as a function of pillar interval-to-width ratio. On the original textured Si substrate with hydrophilic pillars, the water droplet possesses a larger apparent CAs ($> 90^\circ$) and contact angle hysteresis (CAH), induced by the hierarchical roughness of microscale pillar arrays and nanoscale pit-like roughness. However, the silanized textured substrate shows superhydrophobicity induced by the low free energy OTS overcoat and the hierarchical roughness of microscale pillar arrays, and nanoscale island-like roughness. The largest apparent CA on the superhydrophobic surface is 169.8°. In addition, the wetting transition of a gently deposited water droplet is observed on the original textured substrate with pillar interval-to-width ratio increasing. Furthermore, the wetting state transition is analyzed by thermodynamic approach with the consideration of the CAH effect. The results indicate that the wetting state changed from a Cassie state to a pseudo-Wenzel during the transition.

Keywords: superhydrophobicity, wetting state transition, textured silicon substrate, thermodynamic method

PACS: 68.08.Bc, 68.35.Md, 81.16.Rf, 81.16.Dn **DOI:** 10.1088/1674-1056/22/10/106801

1. Introduction

As the size of a device shrinks to micro/nanoscale, the effects of surface forces such as adhesion, friction, and surface tension become increasingly critical and dominate over inertial, electromagnetic, and gravitational forces.[1] Excessive adhesive force between the working surfaces is the major cause of the micro/nanoscale device failure.[2,3] On the micro/nanoscale, menisci form around the contacting or near-contacting asperities due to the surface energy effects in the presence of a thin liquid film, or the capillary condensation in the presence of water vapor, which result in high adhesion and friction.[4] As a result of this, functional materials of non-wetting are the desideratum for reducing the micro/nanoscale wear and failure.

The wettability of a solid surface could be characterized by the contact angle (CA), the angle that is included between the solid–liquid and the liquid–air interfaces.[5] The CA depends on several factors, such as energy, roughness, the manner of surface preparation, etc.[6] If water wets the solid surface (referred to as a hydrophilic surface), the value of CA is $0^\circ \leq \theta < 90^\circ$; whereas if water cannot wet the surface (referred to as a hydrophobic surface), the value of CA is $90^\circ \leq \theta \leq 180^\circ$. The fluidity of water droplets on a solid surface is characterized by the contact angle hysteresis (CAH), which is the difference between the advancing and receding CAs. A surface with a high CA ($> 150^\circ$) and a low CAH ($< 5^\circ$) is called a superhydrophobic surface,[7] which attracts extensive attention[8–12] because of the self-cleaning and antisticking properties.[13,14] The superhydrophobicity is mainly determined by the physicochemical property and the surface topography,[15] therefore, the fabrication of a superhydrophobic surface is commonly via two kinds of approaches: one is to modify a rough surface by materials with low surface free energy, and the other is to create a rough structure on a hydrophobic surface.[16–20] By comparison with the low surface free energy, the rough structure is recognized as playing a more important role in creating superhydrophobicity.[21–24] Furthermore, a composite hierarchical rough structure of microscale and nanoscale roughness is considered to be optimized for superhydrophobicity and creating functional devices.[25–28] However, Guo and Liu[29] pointed out that the hierarchical structure is not a necessary condition for the superhydrophobic surface in nature. In addition, the hierarchical roughness could be used for increasing adhesive forces, which is inspired by the gecko toe attachment system.[30] The general method of fabricating the composite hierarchical structures is complicated, and the relationship between the wetting behavior and the roughness dimension is hard to analyze quantitatively due to the irregular shape of the roughness.

On a rough solid surface, there are two wetting states of

*Project supported by the Program for New Century Excellent Talents in University of Ministry of Education of China (Grant No. NCET-09-0211) and the Fundamental Research Funds for the Central Universities (Grant Nos. 2012YJS105 and M13JB00240).

†Corresponding author. E-mail: zhhzhang@bjtu.edu.cn

© 2013 Chinese Physical Society and IOP Publishing Ltd

a liquid droplet. When a liquid droplet suspends above the topography, the air is trapped between the droplet bottom surface and the solid surface. Therefore, the composite interface is formed, and the wetting state is Cassie state.[31] On the other hand, if a liquid droplet wets both the top and bottom of the topography, i.e., the liquid follows the solid surface, the wetting state is Wenzel state, and the homogeneous interface is formed.[32] However, wetting states may not be static, and a wetting transition from a Cassie state to a Wenzel state could occur on a rough surface. The wetting state transition makes the composite interface irreversibly transformed into the homogeneous interface, thus damaging the superhydrophobicity and the relevant functions. Several approaches have been proposed to explain the wetting transition between Cassie state and Wenzel state, including the approach based on the surface geometry,[33] the balance between the body force and the surface force,[34] and the external stimuli, such as pressure and vibration,[35,36] bouncing or evaporation of droplets,[37] to surmount the energy barrier between the two states. However, the main interest in the recent research is in the hydrophobic and superhydrophobic cases. These critical conditions of wetting transition almost fail to apply to a hydrophilic surface. Moreover, the transition on hydrophilic substrates has rarely been discussed experimentally and theoretically except for a few investigations;[38,39] as a result, there has been no convincing explanation of the wetting transition mechanism on the hydrophilic surfaces.

In the present work, the textured Si substrates are decorated with regular microscale square pillar arrays. By the simple modification with self-assembly octadecyltrichlorosilane (OTS)[40] film, the textured Si substrates obtain the superhydrophobicity. The CA measurements and micro/nanoscale hierarchical rough models are used to analyze the relationship between the wetting behavior and the pillar dimension. Particularly, the wetting transition from a Cassie state to a pseudo-Wenzel state induced by the pillar dimension is observed on the original textured substrates with hydrophilic pillars. It is analyzed by thermodynamic approach with the consideration of the CAH effect. The theoretical arguments are well supported by our experimental data.

2. Experimental details

2.1. Materials

Silicon wafers 4 inches in diameter are purchased from China Electronics Technology Group Corporation No. 46 Research Institute. Chloroform ($CHCl_3$, 99.8%), acetone (C_3H_6O, 99.0%), ethanol (C_2H_5OH, 99.0%), sulfuric acid (H_2SO_4, 98%), hydrogen peroxide (H_2O_2, 35%), and hydrofluoric acid (HF, 40%) are purchased from Sinopharm Chemical Reagent Co., Ltd. (Beijing, China). Octadecyltrichlorosilane (OTS, 95%) is bought from J & K Scientific Co. (China). Deionized water (18 Ω/cm) was used in the whole experimental process. All reagents were used without further purification.

2.2. Preparation of superhydrophobic surface

Inductively coupled plasma (ICP) is a familiar way of patterning Si. Microscale square pillar arrays with various dimensions on Si wafer were etched in an STS ASE ICP system (ICP, STS Multiplex ASE-HRM ICP Etcher, STS Ltd., England) using C_4F_8/SF_6 gases. The textured samples were cleaned and hydroxylated by immersing them into a piranha solution (mixture of sulfuric acid and hydrogen peroxide, $H_2SO_4/H_2O_2 = 7:3$ V/V) at 90 °C for 30 min and rinsed thoroughly with deionized water and dried in an N_2 flow. The freshly prepared textured samples were immersed into a 0.2% (V/V) solution of OTS in chloroform ($CHCl_3$) in ambient atmosphere at room temperature (20 °C) for 12 h. The modified samples were successively ultrasonically cleaned with chloroform, acetone, and ethanol and afterwards dried in an N_2 flow.

2.3. Instrumentation

The surface morphologies of the textured Si substrates were investigated by scanning electronic microscope (SEM, Quanta200 FEG, FEI Ltd., Netherlands), and the dimensions of pillar side length, height, and interval were evaluated by SEM and laser scanning confocal microscope (LSCM, LEXT OLS4000, Olympus Ltd., Japan). The topographies of original Si surface and self-assembly OTS film on Si substrate were analyzed by atomic force microscope (AFM, Dimension V, Veeco Ltd., USA).

Contact angle measurements were conducted with deionized water on a CA meter by the sessile drop method. The deionized water droplets of ~ 2 μL were gently deposited on the samples by micro syringe, and the CAs were measured at five different points of each sample. CAH were measured by dropping a water droplet on the sample positioned on a tilting stage. The tilting angle of the stage was adjusted by a micrometer. All the measurements were carried out at room temperature (20 °C) with the relative air humidity of 45%.

3. Results and discussion

3.1. Microscopy of the original and OTS modified textured Si substrates

The SEM micrographs of square pillars with nearly the same side length a_m, height H_m, but various values of interval b_m on Si substrates are shown in Fig. 1. The top view and three-dimensional (3D) micrographs of textured Si substrates are indicated, showing that the pillar surfaces are flat, and side walls in each pillar are straight and almost perpendicular to the substrate. The pillar geometric parameters on each sample are listed in Table 1.

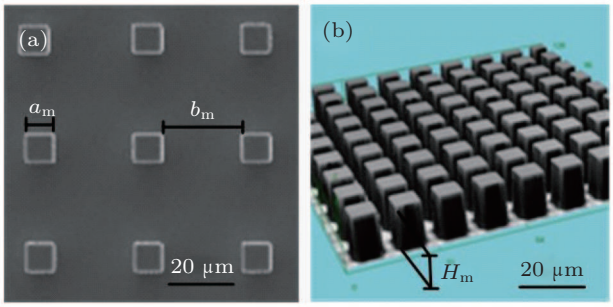


Fig. 1. (color online) Micrographs of textured Si substrate with square pillars of size $a_m \times a_m$, interval b_m, and height H_m in a regular array. Panel (a) shows the top view of SEM micrograph and panel (b) displays the 3D micrograph.

Careful examinations of the original Si substrate, original and OTS modified pillar surfaces were taken by AFM. As shown in Fig. 2(a), the original Si surfaces are unsmooth but with irregularly distributed pits, which were probably generated by the process of ICP etching. Figure 2(b) shows the line sections of pits *a* and *b* in Fig. 2(a). The average dimensions of the pit-like rough structure are ∼ 50 nm in diameter, ∼ 0.6 nm in depth, and ∼ 130 nm in pitch. By contrast, the OTS film overcoating onto Si substrate generates a rough surface consisting of randomly distributed islands as shown in Fig. 3. The top view and 3D micrographs are shown in Figs. 3(a) and 3(b), respectively. Figure 3(c) shows the line sections of islands *a* and *b* in Fig. 3(a). The average dimensions of island-like rough structure are ∼ 70 nm in diameter, ∼ 5 nm in height and ∼ 95 nm in pitch. With the combination of microscale pillars and nanoscale pit-like or island-like roughness, the hierarchical rough structures are formed on the substrate.

Table 1. Geometric parameters of pillar arrays with different dimensions.

Data point	Original design/μm			Measurement/μm			
	a_m	b_m	H_m	a_m	b_m	H_m	b_m/a_m
1#	10	5	18	9.396	5.633	16.846	0.6
2#	10	7	18	9.308	7.130	16.493	0.766
3#	10	9	18	9.242	9.427	17.878	1.02
4#	10	10	18	9.154	10.463	17.665	1.143
5#	10	15	18	8.934	15.272	16.892	1.709
6#	10	20	18	8.714	20.135	15.709	2.311
7#	10	25	18	8.978	25.218	15.512	2.809
8#	10	30	18	8.980	30.499	16.298	3.396
9#	10	35	18	8.714	35.510	17.384	4.075

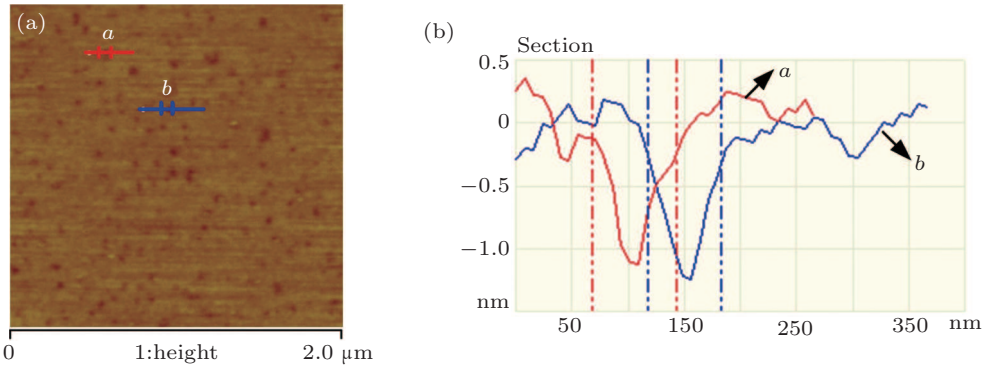


Fig. 2. (color online) AFM topographies of original Si surface. Image (b) is the line sections of image (a), and the scan size is 2 μm×2 μm and the vertical scale is 10 nm.

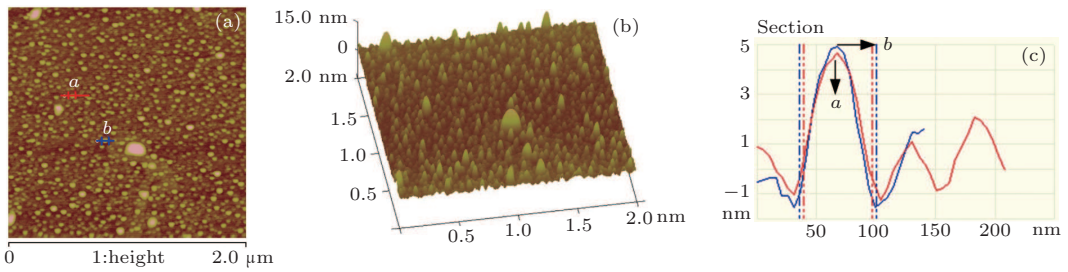


Fig. 3. (color online) AFM topographies of OTS film on Si substrate. Images (a) and (b) are the top view and 3D AFM images, respectively; and image (c) is the line sections of image (a). The scan size is 2 μm×2 μm and the vertical scale is 10 nm.

3.2. Wetting behaviors of water droplet on the prepared substrates

The equilibrium wetting states (Wenzel state and Cassie state) for a droplet on the rough surface are shown in Fig. 4.

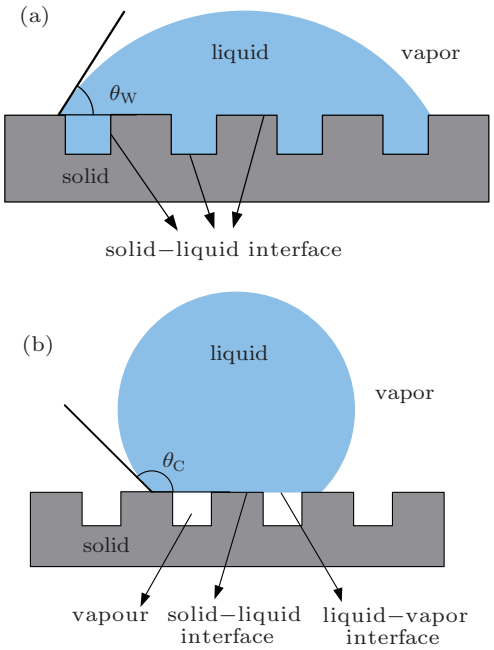


Fig. 4. (color online) Wetting states of a water droplet on the rough surface: (a) Wenzel state and (b) Cassie state.

The apparent CA at the Wenzel state (θ_W) or the Cassie state (θ_C) is given, respectively, as[31,32]

$$\cos\theta_W = r_W \cos\theta_Y, \tag{1}$$

$$\cos\theta_C = r_C \varphi \cos\theta_Y + \varphi - 1, \tag{2}$$

where θ_Y is the CA for smooth surface, θ is the CA for rough surface, r is a roughness factor defined as a ratio of the solid–liquid contact area to its projection on a flat plane, and the subscripts W and C represent the Wenzel and the Cassie states, respectively, and φ is fractional flat geometrical areas of the solid–liquid interface under the droplet. If φ=1, the Cassie regime becomes the Wenzel regime. Based on the hierarchical rough structure model (as shown in Fig. 5), the wetting behaviors of a water droplet on the prepared substrate were theoretically studied. It is assumed that the nanoscale rough structures of radius R_n, projection radius a_n, height H_n, and interval b_n are periodically placed on the pillars. The side views of the Si textured substrates with nanoscale pit-like and island-like roughness are shown in Figs. 5(a) and 5(b), respectively. The top views of microscale and nanoscale rough structures in one period are shown in images (c) and (d), respectively. Moreover, the wetting states on the nanoscale pit-like and island-like roughness are shown in Fig. 6 on the assumption that the pit-like rough structures with low depth-to-width ratio are easily engulfed by liquid.

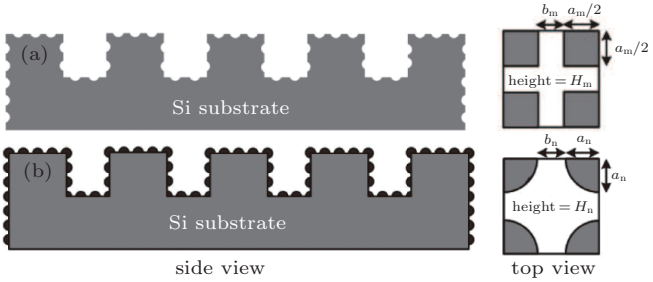


Fig. 5. Schematic illustrations of the hierarchical rough structure models on (a) original and (b) OTS modified textured Si substrate, and (c) microscale and (d) nanoscale roughness in one period.

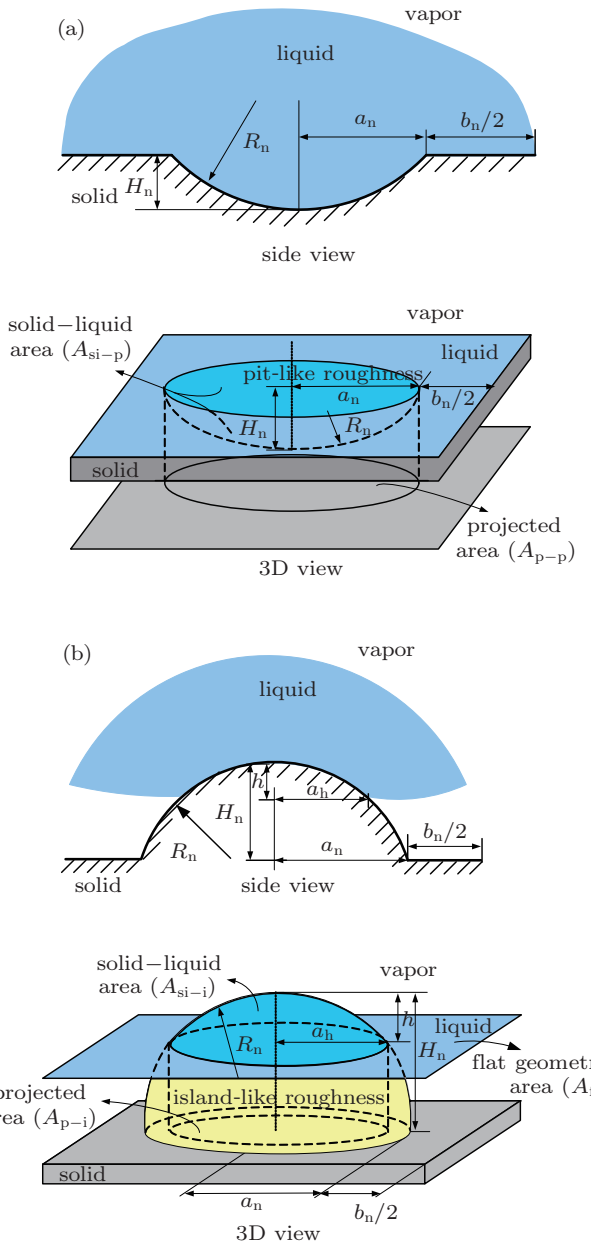


Fig. 6. (color online) Liquid wets the nanoscale (a) pit-like and (b) island-like roughness.

According to the hierarchical rough structure models above, parameters r_W, r_C, and φ are given as

$$r_W = r_m r_p, \tag{3}$$

$$r_{\mathrm{C}} = r_{\mathrm{i}}, \tag{4}$$

$$\varphi = \varphi_{\mathrm{m}}\varphi_{\mathrm{h}}, \tag{5}$$

where

$$r_{\mathrm{m}} = 1 + \frac{4a_{\mathrm{m}}H_{\mathrm{m}}}{(a_{\mathrm{m}}+b_{\mathrm{m}})^2}, \tag{6}$$

$$\varphi_{\mathrm{m}} = \frac{1}{(1+b_{\mathrm{m}}/a_{\mathrm{m}})^2}, \tag{7}$$

$$r_{\mathrm{p}} = \frac{A_{\mathrm{sl-p}}}{A_{\mathrm{p-p}}} = \frac{2R_{\mathrm{n}}H_{\mathrm{n}}}{a_{\mathrm{n}}^2}, \tag{8}$$

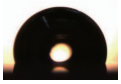
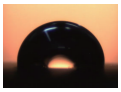
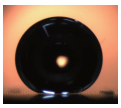
$$r_{\mathrm{i}} = \frac{A_{\mathrm{sl-i}}}{A_{\mathrm{p-i}}} = \frac{2R_{\mathrm{n}}h}{a_{\mathrm{h}}^2}, \tag{9}$$

$$\varphi_{\mathrm{h}} = \frac{A_{\mathrm{sl-i}}}{A_{\mathrm{f}}} = \frac{\pi a_{\mathrm{h}}^2}{(2a_{\mathrm{n}}+b_{\mathrm{n}})^2}, \tag{10}$$

where r_{m}, r_{p}, and r_{i} are the roughness factors of microscale pillar, nanoscale pit-like, and island-like rough structure, respectively; φ_{m} and φ_{h} are fractional flat geometrical areas of the solid–liquid interface under the droplet for microscale pillar and nanoscale island-like rough structure, respectively; both h and subscript h represent the height from the top of the nanoscale rough structure to the liquid–vapor interface. The solid–liquid interface areas $A_{\mathrm{sl-i}}$ (island-like roughness), $A_{\mathrm{sl-p}}$ (pit-like roughness) and their projected areas $A_{\mathrm{p-i}}$ and $A_{\mathrm{p-p}}$ are indicated in the 3D views in Fig. 6. A_{f} is the flat geometrical area. If the liquid droplets thoroughly wet the island-like rough structures, we have $h = H_{\mathrm{n}}$, $\varphi_{\mathrm{h}} = 1$, and $a_{\mathrm{h}} = a_{\mathrm{n}}$.

The wetting behaviors of the original and OTS modified textured Si substrates were experimentally studied by CA measurements. In Table 2, a series of water droplets on the original and OTS modified flat and textured Si substrates, as well as the associated apparent CAs, CAHs, and pillar dimensions are presented. As shown in Table 2, a water droplet on the original textured Si substrates shows a larger apparent CA ($> 90°$) but a high CAH induced by the microscale pillar arrays and the nanoscale pit-like roughness. By comparison, the OTS modified textured Si substrate exhibits extremely high repellency against water droplet. The CA of water droplet is $\sim 170°$ and the CAH is $\sim 3°$. With the synergy effect of hierarchical rough structures and the low surface free energy of the OTS film (CA = 107.38°), the as-prepared OTS modified textured Si substrates obtain the superhydrophobic properties.

Table 2. Apparent CAs and CAHs on the original and OTS modified flat and textured Si substrates.

	Images of water droplets	a_{m}/μm	b_{m}/μm	φ_{m}	Apparent CA	CAH
Original Si substrate		0	0	1	55.13°	> 90°
OTS modified flat substrate		0	0	1	107.38°	50°
Original textured Si substrate		8.714	35.51	0.039	97.58°	65°
OTS modified textured Si substrate		8.714	35.51	0.039	169.8°	3°

In order to reveal the relationship between the wetting behavior and the pillar dimension, the CAs each as a function of $b_{\mathrm{m}}/a_{\mathrm{m}}$ are plotted in Fig. 7, and the experimental data are compared with Cassie equation (Eq. (2)) based on the hierarchical rough models (Fig. 6). Figures 7(a) and 7(b) show the variations of CA with the increase in $b_{\mathrm{m}}/a_{\mathrm{m}}$ on the original and OTS modified textured Si substrates, respectively. On the original textured substrates, there are two stages of the CA variation. In the first stage, with $b_{\mathrm{m}}/a_{\mathrm{m}}$ increasing from 0.6 to 1.02, the apparent CA increases gradually from 130.8° to 149.6°. According to the Cassie theoretical model,[31] the apparent CA of a water droplet on rough surface increases due to the increase in air pocket, despite the primary surface wettability. With the increase in $b_{\mathrm{m}}/a_{\mathrm{m}}$, the solid–air interface becomes larger, and the variation tendency accords well with the Cassie model. Therefore, the wetting states on the textured substrates 1, 2, and 3 are likely to be Cassie states. The measured CAs are larger than the theoretical values of the Cassie regime. Though efforts to explain the exact mechanism of this difference are still under way, a plausible explanation can be given: the contributions come from the disconnected liquid-solid-air triple contact line, sharp edges of the pillars, and the large CAH of the hydrophilic substrate. The apparent CAs on rough substrates are obtained when the water droplet achieves a dynamic equilibrium wetting state. In the wetting progress, the contact line moves across the tops of the asperities. The classical theoretical rough model proposed by Cassie and Baxter[31] is a roughly cylindrical structure. On such surfaces, the contact line is continuous, and the water droplet is considered to spread readily. Therefore, the equi-

librium wetting state and the true apparent CAs are easier to obtain. In contrast, the pillar-like structures are disconnected, which leads to the disconnection of the contact lines, and the contact lines could be easily pinned on the sharp edges and the corners of pillars in the wetting progress. Moreover, due to the hydrophilicity of the pillars, the CAH of the water droplet is large. From the above, a water droplet is so unfavorable to spread that the apparent CAs are larger than the theoretical values of the Cassie regime on the original textured substrate. In the second stage, as b_m/a_m turns larger than 1.02, the apparent CA starts to decrease, which indicates that there is a beginning of wetting state transition with the increase in b_m/a_m. At this time, the water droplet wets not only the tops but also the side walls of pillars. The wetting state after the wetting transition is worthy to be discussed. Based on the intruding angle criterion proposed by Wang and Chen,[41] air cannot be entrapped in the hydrophilic pillars with an intruding angle less than or equal to 90°. Therefore, the metastable Cassie state cannot be realized on the original textured substrate with hydrophilic pillars. According to the Wenzel theoretical model, the hydrophilicity is enhanced, i.e., the apparent CA decreases, by the rough structure on the primary hydrophilic surface.[32,33] However, the apparent CA of original Si surface is 55.13°, which implies that the original Si surface is more hydrophilic than the textured surface with pillar arrays. Therefore, the wetting state on the textured substrate with b_m/a_m larger than 1.02 might be a pseudo-Wenzel state. At the pseudo-Wenzel state,[38] the water droplet wets both the tops and the bottoms of the rough structure as a Wenzel droplet; however, due to the pinning of the contact line by sharp edges of pillars and the large CAH on the hydrophilic surface, the wetting area projected on the horizontal plane is smaller and the apparent CA is larger than the theoretical values of the Wenzel regime, respectively.

On the OTS modified substrates, the apparent CAs are larger than 150°, and the CAHs are nearly 3° ∼ 5°. Apparent CAs on such substrates increase with the increase in b_m/a_m, and are closer to the values predicted by Cassie regime. Furthermore, the variation tendency accords well with the Cassie model. With the synergy effect of low surface free energy and the hierarchical roughness, there is a stable composite interface between the water droplet, micro/nano hierarchical rough structures, and the entrapped air pockets. Therefore, water droplets stay at stable Cassie state and the wetting state transition will not occur. The low free energy of OTS film and the island-like nanoscale roughness dramatically weaken the pinning of the contact line by sharp edges, thereby leading to a lower CAH. The depth-to-width ratio of nanoscale roughness is low, thus the water droplet is considered to be easy to engulf part of the nanoscale islands. For this reason, there is a difference between the experimental and theoretical results obtained by Cassie regime.

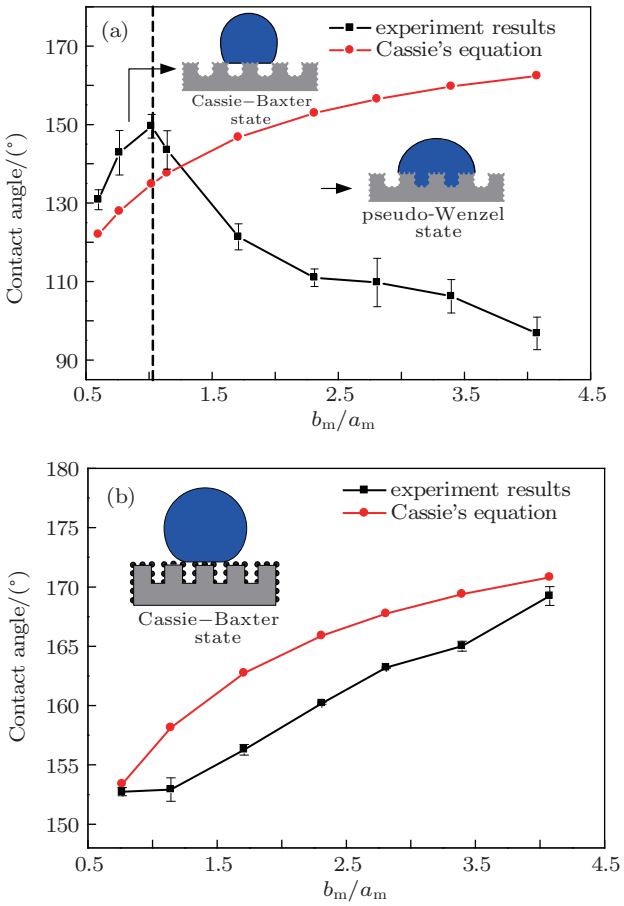


Fig. 7. (color online) Apparent CAs of water drops deposited on the (a) original and (b) OTS modified textured Si substrate, each as a function of b_m/a_m. Theoretical lines of the Cassie–Baxter wetting regime (Eq. (2)) and the experimental data are denoted with solid circles and solid squares, respectively.

3.3. Wetting state transition on the original textured substrate

On the OTS modified textured substrate, water droplets always stay in a stable Cassie state (as shown in Fig. 7(b)); however, on the original textured substrate, the wetting transition from a Cassie state to a pseudo-Wenzel state, induced by the pillar dimension, is observed (as shown in Fig. 7(a)). In the CA measurements, the wetting process of a water droplet could be observed on the original textured substrate with a larger pillar interval. As shown in Fig. 8(a), the gently deposited water droplet is found to contact only the tops of the pillars, because the light passing through the grooves of the rough surface could be seen clearly, indicating that a composite surface was formed. After a few seconds, the water droplet penetrated into the grooves and finally collapsed onto the substrate without any perturbation to the water droplet or the substrate (Fig. 8(b)). As a result, the apparent CA reduced from 154.3° to 109.4°.

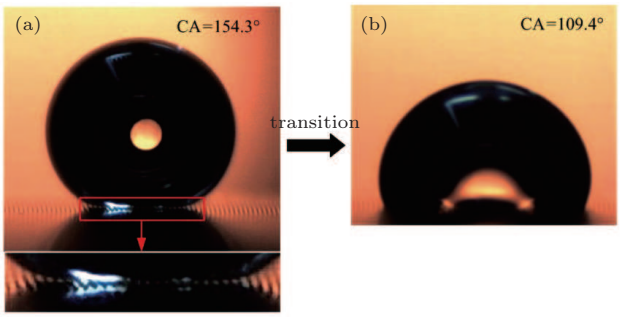


Fig. 8. (color online) Wetting process of a water droplet on the original textured Si substrate with $b_m/a_m = 3.1$. Panel (a) shows a composite droplet and an apparent CA of 154.3°, and panel (b) displays a wetted droplet and an apparent CA of 109.4°.

Assuming that the penetration during the wetting process starts from the center of the droplet bottom, the wetting transition from a Cassie state to a pseudo-Wenzel state is shown in Fig. 9. The penetration state is characterized by the variables x and X, where X is the radius of drop bottom, and x is the radius of the wetted circle in the groove.

Consider a drop on a rough substrate. The surface energy, G, of the drop is presented by[42]

$$G_{C,P}=S_{C,P}\sigma_{lv}-A_{C,P}\cos\theta_{C,W}\sigma_{lv}, \quad (11)$$

$$G_{penetration}=S_C\sigma_{lv}-A_C\cos\theta_C\sigma_{lv}+\pi x^2(\cos\theta_C-\cos\theta_W), \quad (12)$$

where the interfacial area S of the spherical cap is given by

$$S_{C,P}=2\pi R_{C,P}^2(1-\cos\theta_{C,P}), \quad (13)$$

the area A of contacting the substrate projected on the horizontal plane can be written as

$$A_{C,P}=\pi R_{C,P}^2\sin^2\theta_{C,P}, \quad (14)$$

σ_{lv} is the surface tension on the liquid–vapor interface, R is the radius of the spherical droplet, and the subscripts C and P represent the Cassie state and the pseudo-Wenzel state, respectively.

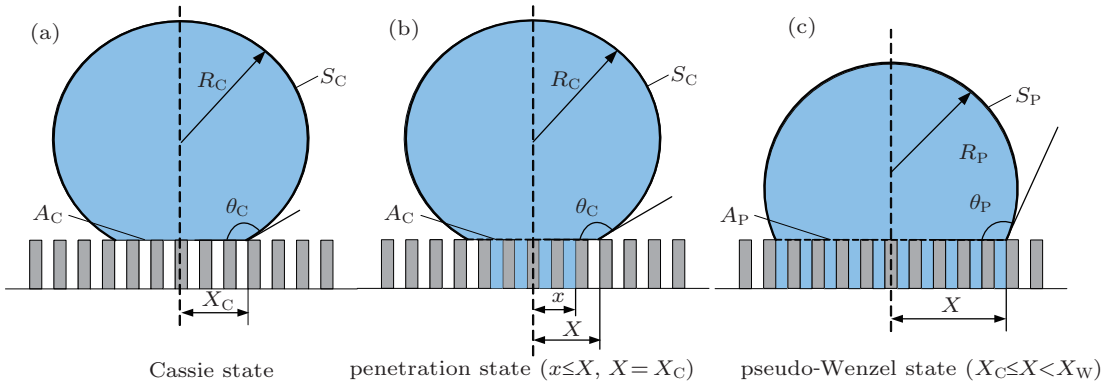


Fig. 9. (color online) Wetting transitions from a Cassie state to a pseudo-Wenzel state for the cases of (a) Cassie state, (b) penetration state, and (c) pseudo-Wenzel state.

Substituting the expressions for S and A into Eqs. (11) and (12), the energies can be written as

$$G_C = \pi^{1/3}(3V)^{2/3}\sigma_{lv}(2-3\cos\theta_C+\cos^3\theta_C)^{1/3}, \quad (15)$$

$$G_{Penetration} = \sigma_{lv}\pi\left(\frac{2X_C^2}{1+\cos\theta_C}-X_C^2\cos\theta_C + x^2(\cos\theta_C-\cos\theta_W)\right), \quad (16)$$

$$G_P = \pi^{1/3}(3V)^{2/3}\sigma_{lv}(2-3\cos\theta_P+\cos^3\theta_P)^{-2/3} \times(2-2\cos\theta_P-\sin^2\theta_P\cos\theta_W), \quad (17)$$

where V is the droplet volume, X_C is the radius of the bottom of a Cassie droplet cap, and θ_P is the CA in the pseudo-Wenzel state.

With the large CAH of the hydrophilic substrate, the hysteresis energy cannot be ignored during the wetting transition. If the droplet stays in the penetration state ($x \le X_C$), the hysteresis energies are given by[38]

$$G_S=\pi\gamma\delta(r_m-1)x^2, \quad (18)$$

$$G_L=\pi\gamma\delta(1-\varphi_m)x^2, \quad (19)$$

where, G_S is the hysteresis energy, when the contact line moves down along the side wall of the pillars; while G_L is the hysteresis energy, when the contact line moves along the level surface of top pillars or the bottom substrates; $\delta = |\cos\theta_{adv}-\cos\theta_{rec}|$, with θ_{adv} and θ_{rec} being the advancing CA and receding CA, respectively. If the droplet stays in the pseudo-Wenzel state ($x = X > X_C$), the hysteresis energy can be estimated as:

$$G_S = \pi\gamma\delta(r_m-1)X^2, \quad (20)$$

$$G_L = \pi\gamma\delta(1-\varphi_m)X_C^2+\pi\gamma\delta(X^2-X_C^2). \quad (21)$$

The total energy in the penetration state is given by $G_T=G_{Penetration}+G_S+G_L$. Assume that the gravity effects do not play a significant role in the wetting transition, and the wetting state and the CA are determined by the equilibrium between the G_C and the G_T. Under the assumption, the relation between the energy and the x/X_C ratio is shown in Fig. 10.

As the water droplet starts to penetrate the grooves, x increases and the energy decreases. However, the increasing hysteresis energy during the wetting will prevent the contact line from moving, so that the water droplet could be imprisoned on the substrate. As shown in Fig. 10(a), with the increase in x/X_C, the energy increases for samples 1, 2, and 3, which indicates that with the increase in x/X_C, the total free energy G_T of penetration state is larger than the initial energy G_C ($x/X_C = 0$). Due to the energy barrier, the wetting transition on such a substrate is energetically unfavorable, which proves that each of the wetting states of droplets on samples 1, 2, and 3 is Cassie state as discussed in Subsection 3.2. Specifically, energy first decreases and then increases with the increase in x/X_C for sample 4, which indicates that the water droplet first penetrates into the grooves and then is stopped by the hysteresis energy barrier. That is the reason why the CA on sample 4 does not continue to increase with the increase in b_m/a_m (Fig. 7(a)). As shown in Fig. 10(b), G_C ($x/X_C = 0$) are larger than G_T for samples 5–9, indicating that each of the water droplets on such samples could not stay in a penetration state, but continue to spread on the substrates. The results give an explanation of the sharp decrease in the CA on each of samples 5–9 in our experiments as shown in Fig. 7(a).

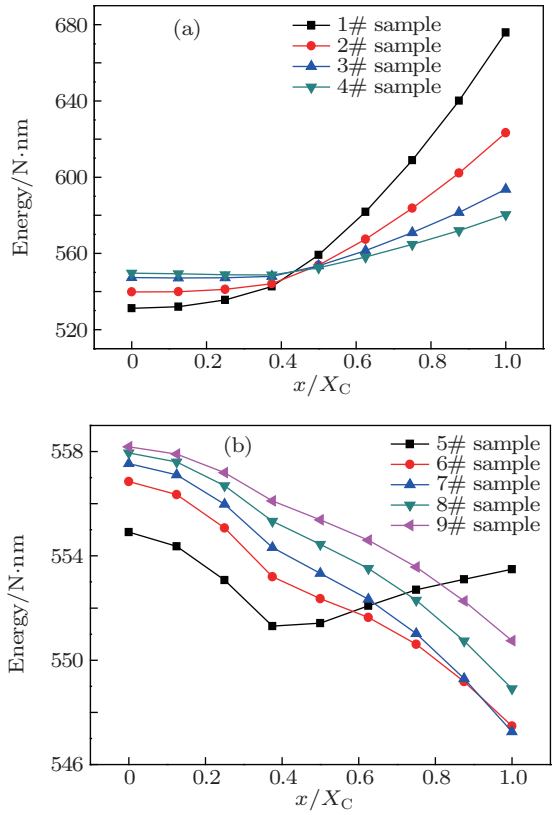


Fig. 10. (color online) Relations between the energy and x/X_C for (a) samples 1–4, and (b) samples 5–9.

With the increase in X, the wetting state changes from pseudo-state to Wenzel state as seen in Fig. 9(c). The relations between CA and the radius of drop cap bottom X for samples 5–9 are shown in Fig. 11. In the wetting process, X turns larger, thereby leading to a decrease in CA for each sample, and the equilibrium CA on each sample is obtained when $G_C = G_P + G_S + G_L$. As shown in Fig. 11, the experimental CA is larger than the equilibrium CA for each sample. This is because of ignoring the pinning effect on the contact line by sharp edges during the wetting transition. The roughness r_m continues to decrease from sample 5 to 9, indicating that the pinning effects on those samples decrease in sequence. Therefore, the difference between the experimental CA and the equilibrium CA also decreases successively. Even though the water droplets on such samples stay in the equilibrium state, the equilibrium CAs are all larger than the Wenzel CAs. This proves that the wetting states for such samples are each pseudo-Wenzel state.

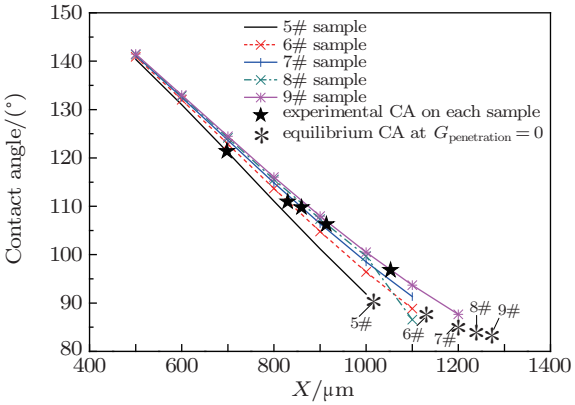


Fig. 11. (color online) Relations between CA and X for samples 5−9, where the solid pentacles (★) and the asterisks (∗) represent the experimental CAs and the equilibrium CAs on each sample, respectively.

4. Conclusion

Microscale pillar arrays are prepared on the Si substrate. The wetting behaviors of original textured substrates and OTS modified ones are analyzed by CA measurements. With the synergy effect with the low surface free energy and the composite hierarchical rough structure of microscale and nanoscale roughness, OTS modified textured substrates obtain the superhydrophobicity. On such substrates, water droplets always stay in the Cassie state. On the original textured substrates, wetting transition from a Cassie state to a pseudo-Wenzel state is found with the increase in pillar interval-to-width ratio. The wetting state transition on hydrophilic surface is thermodynamically analyzed with the consideration of the CAH effect. This approach provides the evidence of the existence of Cassie/pseudo-Wenzel state before/after the wetting transition, and is helpful in understanding the wetting state transition process on hydrophilic rough surface.

References

[1] Jung Y C and Bhushan B 2008 *J. Microsc.* **229** 127
[2] Liu S S, Zhang C H and Liu J M 2010 *Acta Phys. Sin.* **59** 6902 (in Chinese)
[3] Cai S B and Bhushan B 2008 *Mater. Sci. Eng. R* **61** 78
[4] Butt H J and Kappl M 2009 *Adv. Colloid Interface Sci.* **146** 48
[5] Nosonovsky M 2007 *Langmuir* **23** 3157
[6] Adamson A W 1990 *Physical Chemistry of Surfaces* (New York: John Wiley & Sons)
[7] Nosonovsky M and Bhushan B 2007 *Ultramicroscopy* **107** 969
[8] Koch K and Barthlott W 2009 *Phil. Trans. R. Soc. A* **367** 1487
[9] Patankar A N 2004 *Langmuir* **20** 8209
[10] Feng X J and Jiang L 2006 *Adv. Mater.* **18** 3063
[11] Erbil H Y, Demirel A L, Avci Y and Mert O 2003 *Science* **299** 1377
[12] Tuteja A, Choi W, Ma M L, Mabry M J, Mazzella A S, Rutledge C G, Mckinley H G and Cohen E R 2007 *Science* **318** 1618
[13] Lee S M and Kwon T H 2006 *Nanotechnology* **17** 3189
[14] Bhushan B, Nosonovsky M and Jung Y C 2007 *J. R. Soc. Interface* **4** 643
[15] Yang Z, Xu X L, Gong M G, Liu L and Liu Y S 2010 *Chin. Phys. B* **19** 126103
[16] Genzer J and Efimenko K 2000 *Science* **290** 2130
[17] Sun M H, Luo C X, Xu L P, Ji H, Ouyang Q, Yu D P and Chen Y 2005 *Langmuir* **21** 8978
[18] Zhai L, Cebeci F C, Cohen R E and Rubner M F 2004 *Nano Lett.* **4** 1349
[19] Lim J A, Cho J H, Jang Y, Han J T and Cho K 2006 *Thin Solid Films* **515** 2079
[20] Im M, Im H, Lee J H, Yoon J B and Choi Y K 2010 *Langmuir* **26** 17389
[21] Nishino T, Meguro M, Nakamae K, Matsushita M and Ueda Y 1999 *Langmuir* **15** 4321
[22] Salvadori M C, Cattani M, Oliveira M R S, Teixeira F S and Brown I G 2010 *J. Appl. Phys.* **108** 024908
[23] Zhu M F, Zuo W W, Yu H, Yang W and Chen Y M 2006 *J. Mater. Sci.* **41** 3793
[24] F urstner R and Barthlott W 2005 *Langmuir* **21** 956
[25] Gong M G, Xu X L, Yang Z, Liu Y S and Liu L 2010 *Chin. Phys. B* **19** 056701
[26] Guo Z, Chen X, Li J, Liu J H and Huang X J 2011 *Langmuir* **27** 6193
[27] Liu H H, Zhang H Y and Li W 2011 *Langmuir* **27** 6260
[28] Zhao X W, Jiang P, Gao Y, Wang J X, Song L, Liu D F, Liu L F, Dou X Y, Luo S D, Zhang Z X, Xiang Y J, Zhou W Y and Wang G 2005 *Chin. Phys.* **14** 1471
[29] Guo Z G and Liu W M 2007 *Plant Science* **172** 1103
[30] Autumn K 2007 *MRS Bull.* **32** 473
[31] Cassie A B D and Baxter S 1944 *Trans. Faraday. Soc.* **40** 546
[32] Wenzel R N 1936 *Ind. Eng. Chem.* **28** 988
[33] Ran C B, Ding G Q, Liu W C, Deng Y and Hou W T 2008 *Langmuir* **24** 9952
[34] Extrand C W 2002 *Langmuir* **18** 7991
[35] Lafuma A and Quere D 2003 *Nat. Mater.* **2** 457
[36] Bormashenko E, Pogerb R, Whyman G and Erlich M 2007 *Langmuir* **23** 6501
[37] Nosonovsky M and Bhushan B 2008 *Langmuir* **24** 1525
[38] Ishino C and Okumura K 2008 *Eur. Phys. J. E* **25** 415
[39] Whyman G and Bormashenko E 2011 *Langmuir* **27** 8171
[40] Lin L Y, Kim H J and Kim D E 2008 *Appl. Surf. Sci.* **254** 7370
[41] Wang J D and Chen D R 2008 *Langmuir* **24** 10174
[42] Patankar N A 2003 *Langmuir* **19** 1249